Turbulent cascade, bottleneck and thermalized spectrum in hyperviscous flows

Rahul Agrawal, Alexandros Alexakis, Marc Brachet, Laurette S. Tuckerman

Turbulent cascade, bottleneck and thermalized spectrum in hyperviscous flows

Rahul Agrawal
Department of Mechanical Engineering, Indian Institute of Technology Bombay, Maharashtra, India 400076

Alexandros Alexakis and Marc E. Brachet
Laboratoire de Physique de l'École Normale Supérieure, CNRS, PSL Research University, Sorbonne Université, Université de Paris, F-75005 Paris, France

Laurette S. Tuckerman
Physique et Mécanique des Milieux Hétérogènes (PMMH), ESPCI Paris, CNRS, PSL Research University, Sorbonne Université, Université de Paris, F-75005 Paris, France

(Dated: February 20, 2020)

In many simulations of turbulent flows, the viscous forces $\nu\nabla^2\mathbf{u}$ are replaced by a hyper-viscous term $-\nu_p(-\nabla^2)^p\mathbf{u}$ in order to suppress the effect of viscosity at the large scales. In this work we examine the effect of hyper-viscosity on decaying turbulence for values of p ranging from $p = 1$ (ordinary viscosity) up to $p = 100$. Our study is based on direct numerical simulations of the Taylor-Green vortex for resolutions from 512^3 to 2048^3. Our results demonstrate that the evolution of the total energy E and the energy dissipation ϵ remain almost unaffected by the order of the hyper-viscosity used. However, as the order of the hyper-viscosity is increased, the energy spectrum develops a more pronounced bottleneck that contaminates the inertial range. At the largest values of p examined, the spectrum at the bottleneck range has a positive power-law behavior $E(k) \propto k^\alpha$ with the power-law exponent α approaching the value obtained in flows at thermal equilibrium $\alpha = 2$. This agrees with the prediction of Frisch et al. [Phys. Rev. Lett. 101, 144501 (2008)] who suggested that at high values of p, the flow should behave like the truncated Euler equations (TEE). Nonetheless, despite the thermalization of the spectrum, the flow retains a finite dissipation rate up to the examined order, which disagrees with the predictions of the TEE system implying suppression of energy dissipation. We reconcile the two apparently contradictory results, predicting the value of p for which the hyper-viscous Navier-Stokes goes over to the TEE system and we discuss why thermalization appears at smaller values of p.

PACS numbers: 47.10.A,47.11.Kb,47.15.ki

I. INTRODUCTION

Most planetary and astrophysical flows are highly turbulent. As a result, for a wide range of scales, the viscosity has no direct effect on the flow and so the flow evolves as if it were inviscid. Nonetheless viscosity cannot be neglected because it acts effectively at the smallest scales, converting the coherent energy of the flow into heat. It is thus essential in numerical simulations to resolve all scales: from the large scales, where energy is injected and that follow inviscid dynamics, to the smallest scales, where dissipation takes place. However, even with today's computational power, it is still impossible to achieve a resolution that is sufficient to simulate most atmospheric flows. Various methods have therefore been devised to model the small-scale dissipation in order to follow the inviscid dynamics of the large-scale flows while correctly capturing the dissipation rate at small scales. A popular model for spectral codes is the use of hyperviscosity, meaning that the Laplacian of the standard viscous term is replaced by a higher power of the Laplacian. In this way the portion of the spectral resolution devoted to simulating the viscous wavenumbers is reduced, leaving a larger range of wavenumbers that evolve almost inviscidly. Indeed, hyperviscosity models have been shown to reproduce the turbulent evolution of the large scales, manifesting the Kolmogorov energy spectrum

$$E(k) = C\epsilon^{2/3}k^{-5/3}, \tag{1}$$

where $E(k)$ is the energy spectrum, k is the wavenumber, ϵ is the energy dissipation rate and $C \simeq 1.58$ is the Kolmogorov constant.

However, the statistics of turbulent flows are not unaffected by this change of the dissipation term and various studies have been devoted to analyzing these undesirable effects of hyper-viscosity for fluid turbulence [1–7] and Burgers turbulence [8–10]. In particular, at small scales close to the dissipation range, hyper-viscosity is known to produce an aggravated *bottleneck* effect. The bottleneck effect is an accumulation of the cascading energy at wavenumbers just below the dissipation range, leading to a change in the power-law behavior of the energy spectrum. The bottleneck effect exists even for ordinary viscosity and has been the subject of many studies in turbulence [11–15]. With the use of hyper-viscosity, the bottleneck becomes more pronounced, even leading to a non-monotonic behavior of the energy spectrum. In fact it has been conjectured by Frisch et al. [6] that for sufficiently high order of hyper-viscosity, the bottleneck will take the form of a *thermalized* absolute equilibrium state discussed by Kraichnan [16] in which energy is equally distributed among all Fourier modes, leading to an energy spectrum

proportional to k^2. This thermalized spectrum is realized in the truncated Euler equations, for which the Euler equations are solved in Fourier space while keeping only a finite number of Fourier modes. This system conserves exactly the inviscid quadratic invariants of the system. The argument of [6] for the appearance of the thermalized energy spectrum in hyper-viscous flows is that as the order of the hyper-viscosity is increased to very large values, it suppresses all energy above a wavenumber k_G (determined by the value of the hyper-viscous coefficient) while leaving unaffected all wave numbers below. It thus acts as a Galerkin truncation, similarly to the truncated Euler equations. This result was verified with the use of the EDQNM approximation and more extensively for the one-dimensional Burgers equation [8–10]. However, it has not been verified for the three-dimensional hyper-viscous Navier-Stokes equations.

In this work, we explore further the effect of hyper-viscosity carrying out high-resolution Direct Numerical Simulations (DNS) of the decay of a Taylor-Green vortex. Taking advantage of the symmetries of the Taylor-Green flow [17] and using a slaved time-stepping method [18] we have been able to perform many simulations at different orders of hyper-viscosity, reaching values that are sufficiently high to test the thermalisation conjecture.

II. DEFINITION OF THE SYSTEM

A. Basic definitions

We consider the 3D hyper-viscous incompressible Navier-Stokes equations that control the evolution of the velocity field $\mathbf{u}(x,y,z,t) \in \mathbb{R}^3$ defined in $(x,y,z) \in [0, 2\pi L]^3$ and in a time interval $t \in [0,T)$:

$$\frac{\partial \mathbf{u}}{\partial t} + \mathbf{u}\cdot\nabla\mathbf{u} = -\nabla P - \nu_p(-\nabla^2)^p\mathbf{u}, \tag{2}$$

where incompressibility $\nabla\cdot\mathbf{u} = 0$ is assumed, P is the pressure, p is the order of hyper-viscosity, and ν_p a hyper-viscosity coefficient. The periodicity of $\mathbf{u}$ allows us to use the (standard) Fourier representation

$$\widehat{\mathbf{u}}(\mathbf{k},t) = \frac{1}{(2\pi L)^3}\int_D \mathbf{u}(\mathbf{x},t)\exp(-i\mathbf{k}\mathbf{x})d^3x \tag{3}$$

$$\mathbf{u}(\mathbf{x},t) = \sum_{\mathbf{k}\in\mathbb{Z}^3}\widehat{\mathbf{u}}(\mathbf{k},t)\exp(i\mathbf{k}\mathbf{x}), \tag{4}$$

The kinetic energy spectrum $E(k,t)$ is defined as the sum over spherical shells

$$E(k,t) = \frac{1}{2}\sum_{\substack{\mathbf{k}\in\mathbb{Z}^3 \\ k-1/2<|\mathbf{k}|<k+1/2}} |\widehat{\mathbf{u}}(\mathbf{k},t)|^2, \tag{5}$$

and the total energy is

$$E = \frac{1}{2(2\pi L)^3}\int_D |\mathbf{u}(\mathbf{x},t)|^2 d^3x = \frac{1}{2}\sum_{\mathbf{k}\in\mathbb{Z}^3}|\widehat{\mathbf{u}}(\mathbf{k},t)|^2, \tag{6}$$

The dissipation rate of energy is given by

$$\epsilon = \nu_p\sum_{\mathbf{k}\in\mathbb{Z}^3} k^{2p}|\widehat{\mathbf{u}}(\mathbf{k},t)|^2. \tag{7}$$

As p increases, the dissipation is concentrated at increasingly large wavenumbers. We calculate the dissipation rate as the finite difference $-dE/dt$, since summing the expression (7) would multiply the small error in $E(k)$ by a large factor νk^{2p}.

B. Taylor-Green vortex

The initial condition we consider is the Taylor-Green (TG) vortex [19], which is given by

$$\mathbf{u}^{\mathrm{TG}} = U\begin{bmatrix} +\sin(x/L)\cos(y/L)\cos(z/L) \\ -\cos(x/L)\sin(y/L)\cos(z/L) \\ 0 \end{bmatrix} \tag{8}$$

so that the total energy is given by $E = U^2/8$. We non-dimensionalize by L and U, setting these to 1. Time is scaled by the advective time ($L/U = 1$).

The TG vortex is closely related to the von Kàrmàn (VK) swirling flow that has been the subject of many experimental studies [20–22]. The VK flow and the TG vortex have the same basic geometry: both consist of a shear layer between two counter-rotating circulation cells. The TG vortex, however, is periodic with impermeable free-slip boundaries (present as mirror symmetries) while the experimental flow takes place between two counter-rotating coaxial impellers and is confined inside a cylindrical container. The TG vortex also obeys a number of additional rotational symmetries.

The symmetries of the TG initial conditions (8) are preserved by the time evolution. These are, first, rotations by π around the axes $x = z = \pi/2$ and $y = z = \pi/2$, and by $\pi/2$ around the axis $x = y = \pi/2$. A second set of symmetries corresponds to planes of mirror symmetry: $x = 0,\pi$, $y = 0,\pi L$ and $z = 0,\pi L$. On the symmetry planes, the velocity $\mathbf{u}^{\mathrm{TG}}$ and the vorticity $\boldsymbol{\omega}^{\mathrm{TG}} = \nabla\times\mathbf{u}^{\mathrm{TG}}$ are (respectively) parallel and perpendicular to these planes that form the sides of the so-called impermeable box that confines the flow. It is demonstrated in [23] that these symmetries imply that the Fourier expansion coefficients $\widehat{\mathbf{u}}(m,n,p,t)$ of the velocity field in (4) vanish unless m,n,p are either all even or all odd integers. This can be used to reduce memory storage and speed up computations [24, 25] by a factor of 8. If this symmetry is not imposed, round-off errors can break the symmetries as the flow evolves. However, this bifurcation occurs significantly later than the times considered in the present study.

To simulate the evolution of the Taylor-Green flow we used the TYGRS (TaYlor-GReen Symmetric), a pseudospectral parallel code that enforces the symmetries of the TG vortex in 3D hydrodynamics within the periodic cube of length 2π. Details of the code can be found in [17].

C. Choice of parameters

As the value of p is varied, the value of ν_p must be adjusted accordingly. To attain high Reynolds numbers, ν_p should be as small as possible, subject to the constraint that the simulation be well resolved. To insure adequate resolution, we measured the energy spectrum $E(k)$ at the time of maximum energy dissipation and verified that at large k it follows an exponential law $E(k) \propto e^{-k/k_d}$, with k_d the dissipation wavenumber such that $k_{max}/k_d \geq 2$. Here k_{max} is the maximum wavenumber given by $k_{max} = N/3$ due to dealiasing. The exponential law implies that the grid size is smaller than the hyper-viscous Kolmogorov length-scale $\eta_p = (\nu_p^3/\epsilon)^{1/(6p-2)}$ (where $\epsilon \propto U^3/L$) i.e. that $k_{max}\,\eta_p > 1$. This in turn implies that for a fixed grid size, ν_p should be chosen to have an exponential dependence on p given by $\nu_p \propto UL^{-1/3}k_{max}^{2p-2/3}$. If we define the Reynolds number Re_p to be inversely proportional to the hyper-viscosity as $Re_p = UL^{2p-1}/\nu_p$ then the value that can be achieved for a given resolution is

$$Re_p \propto (k_{max}L)^{2p-2/3}. \tag{9}$$

The high value of p imposes additional demands on the time-integration scheme. Because of this, we used a modified exponential method, also called the *slaved* method [18], which is described in detail in Appendix A.

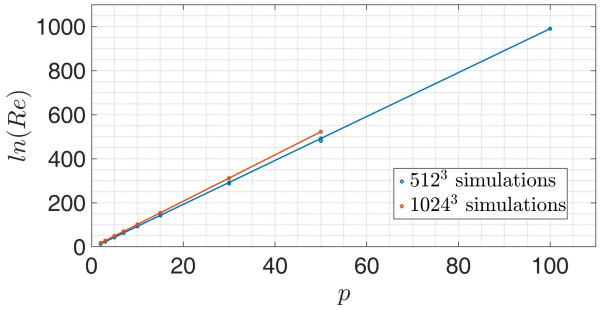

FIG. 1. Reynolds number used in the different runs as a function of the order p of hyper-viscosity.

In the present study, we carry out two series of simulations, one with resolution $N = 512$, and another with resolution $N = 1024$, in which we varied the value of p from 1 to 100 or from 1 to 50, respectively. The scaling (9) of the parameters for our runs is shown in figure 1 for the two resolutions. In addition, we performed a simulation with $p = 1$ at $N = 2048$, which serves as a baseline case with which to compare our hyper-viscous runs.

III. RESULTS

A. Global Dynamics

The top panel of figure 2 shows the evolution of the energy as a function of time from the simulations at resolution $N = 1024$. The bottom panel shows the energy dissipation rate. In both panels, the results are compared with the results from the simulation with ordinary viscosity and the higher numerical resolution $N = 2048$.

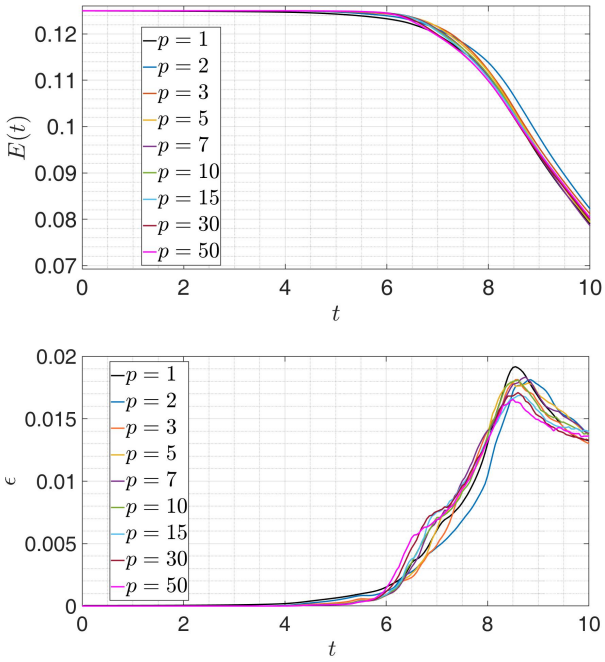

FIG. 2. Top: Time evolution of the total energy for 1024^3 resolution runs for different p values compared to the $p = 1$, $N = 2048$ run. Bottom: mean dissipation rate as a function of time for the same runs.

Surprisingly, even for the largest values of p used, both the energy and the energy dissipation rate are very close to those of the high-resolution run with ordinary viscosity, with the peak dissipation occurring at $t \simeq 8.5$. Thus, despite the very different mechanisms used to dissipate the energy, the global dynamics of the system have not been altered. This indicates that at this resolution, the rate at which energy is dissipated is controlled by the large scale dynamics and the energy cascade and not by the exact dissipation mechanism.

B. Energy Spectra

The global dynamics alone do not, however, guarantee that hyperviscosity correctly models the effect of turbulence at the larger scales. In figure 3, we show in the top panel the energy spectra from the simulation with ordinary viscosity and resolution 2048^3 at eight different

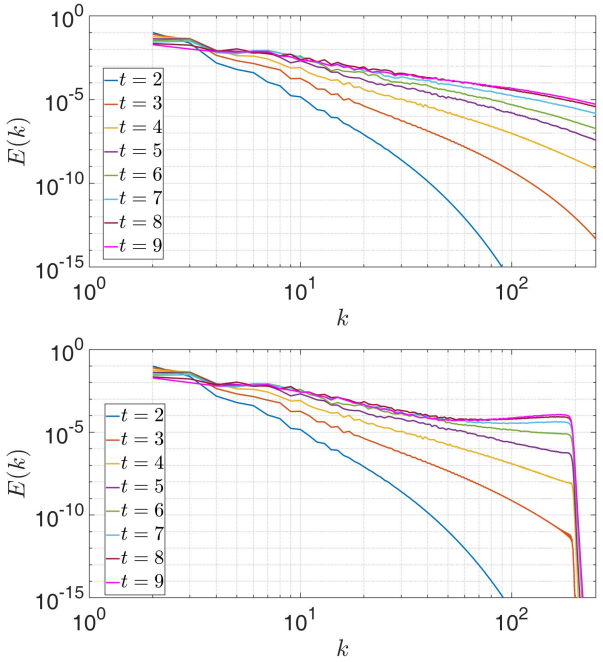

FIG. 3. Energy spectra for the $p = 1$, $N = 2048$ Navier Stokes simulations (top panel) and the $p = 50$, $N = 1024$ simulations (bottom panel).

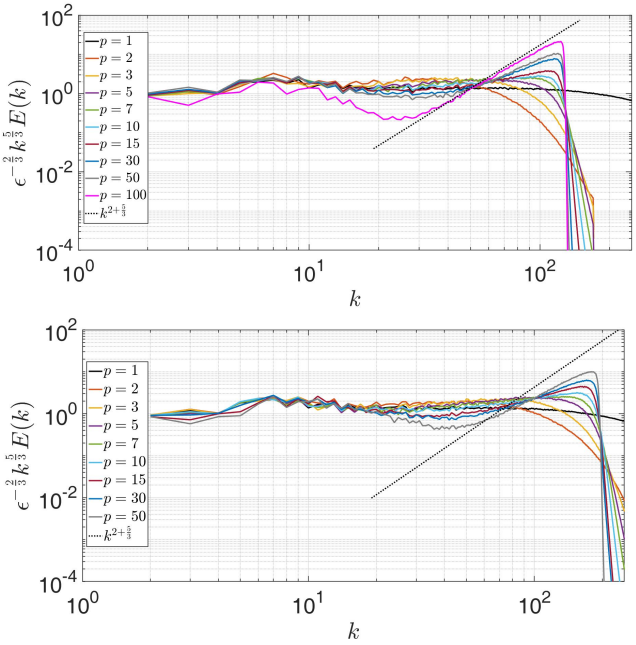

FIG. 4. Top panel: Energy spectra normalized by $k^{-5/3}$ for the 512^3 numerical simulations (top panel) and the 1024^3 simulations (bottom panel).

times, and in the bottom panel the energy spectra from the $p = 50$ simulation at resolution 1024^3. The main and intentional effect of hyperviscosity is clear: there is a very rapid fall-off of the spectrum for $k \gtrsim 190$. Looking at the spectrum for $k \lesssim 190$, the two cases have very similar spectra for times smaller than $t = 5$, for which dissipation effects are negligible, At later times, however, the $p = 50$ runs show an excess of energy at high wavenumbers that becomes more apparent as the peak of the energy dissipation at $t \simeq 8.5$ is approached.

In figure 4 we focus on the time of maximum dissipation and show the energy spectra at this instant for different values of p. The top panel shows the spectra from the 512^3 resolution numerical simulations while the bottom panel shows the results from the 1024^3 simulations. The spectra have been multiplied by $k^{5/3}$ so that a Kolmogorov spectrum would appear as flat. The spectra are surprisingly insensitive to the value of p. For all p, the spectra fall off for $k \gtrsim 130$ for resolution 512^3 and for $k \gtrsim 190$ for resolution 1024^3. The spectra appear close to flat for wavenumbers smaller than $k = 20$. For larger wavenumbers, we observe a dip in the spectrum followed by a bottleneck that becomes stronger as the order of the hyper-viscosity is increased. For large values of p, this bottleneck takes the form of a power-law $E(k) \propto k^{\alpha_p}$ that increases with p.

The dashed line indicates the prediction from thermalization $E(k) \propto k^2$. For each p, we obtained the value of the exponent α_p by fitting the spectrum over the increasing portion of the bottleneck, i.e. for k in the range 50-70 in the 512^3 simulations and 90-110 in the 1024^3 simulations. In figure 5 we show the value α_p as a function of p. We see that as p becomes large, the exponent approaches the thermalized value $\lim_{p\to\infty} \alpha_p = 2$ as predicted in [6].

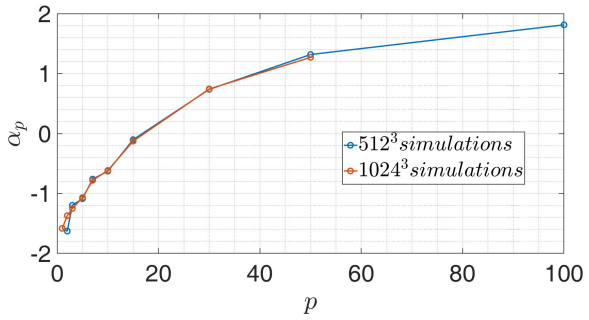

FIG. 5. Measured values of α_p as a function of p for the 512^3 and 1024^3 simulations. The value at $p = 1$ is taken from the 2048^3 simulations.

C. Spatial Structures

We now examine the spatial structure of the flows computed with ordinary and with hyper viscosity. We first recall that the mirror symmetries of the TG vortex with respect to the planes $x = 0, \pi$, $y = 0, \pi$, and $z = 0, \pi$ confine the flow inside the *impermeable box* formed by

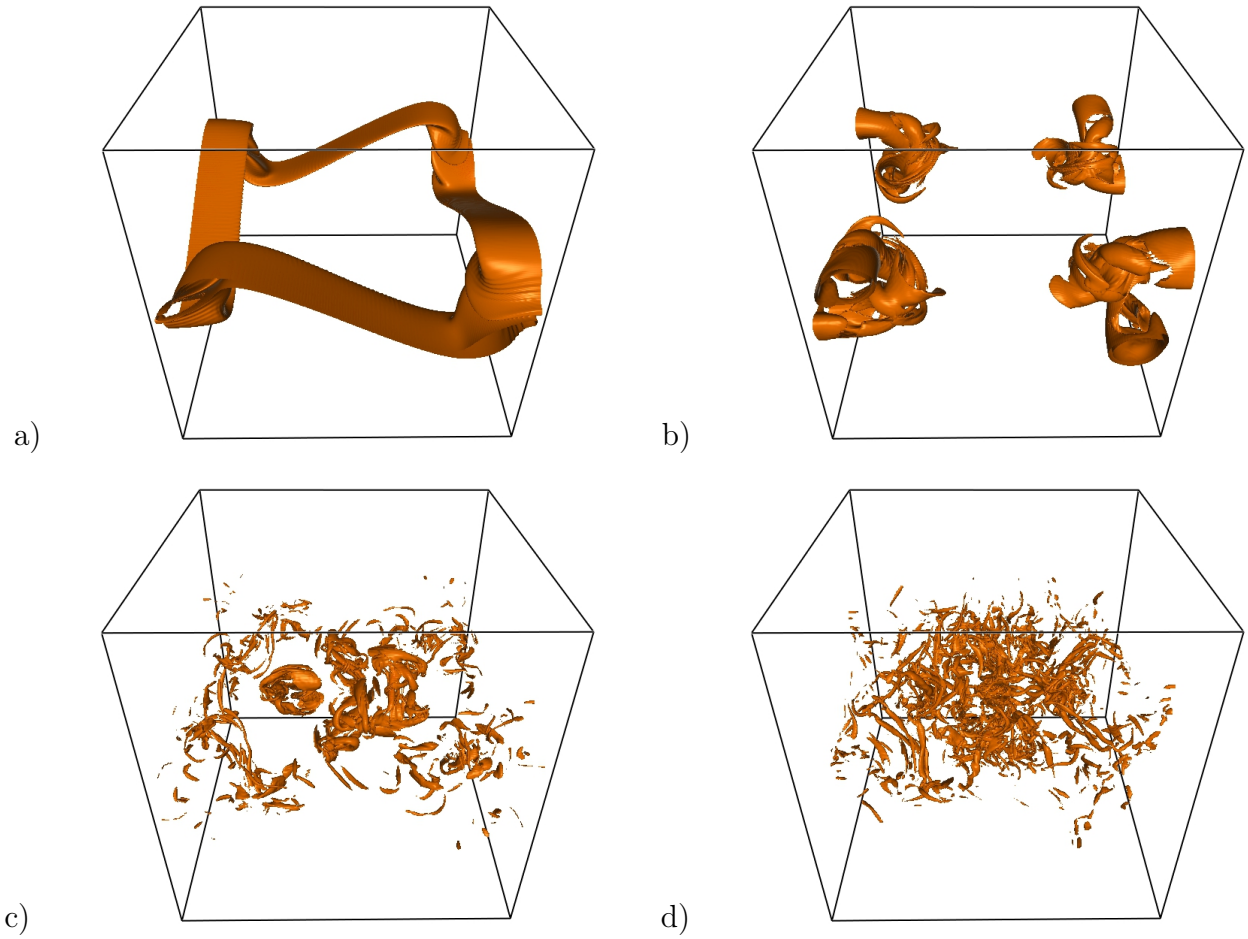

FIG. 6. Isosurfaces (at 8% of maximum) of square vorticity $\omega^2 = (\nabla \times \mathbf{v})^2$ at resolution 512^3 in the impermeable box, with $p = 1$ at $t = 4$, 6, 8, 10.

these planes. The additional rotational symmetries of angle π around the axes $x = z = \pi/2$, $y = z = \pi/2$, and $x = y = \pi/2$ are such that the early-time dynamics can be understood on and near the faces of the impermeable box. Computation of the flow shows that most of the dynamics of the flow for early-to-moderate times ($t < 4$) occurs near these faces. Simple dynamical considerations determine the behavior of the flow on the faces of the impermeable box, resulting in the rapid build-up of a vortex sheet. These considerations determine the dominant features of the flow correctly for times up to about 4. A simple model of this phenomenon is given in appendix D of Brachet et al. [23]. Because of the high Reynolds numbers considered in the present work, for all values of p considered, the dynamics until $t = 4$ is the same and essentially controlled by the inviscid dynamics.

For the standard ($p = 1$) NS equation, when t increases beyond 4, local vorticity maxima develop away from the walls of the impermeable box, suggesting the formation of new daughter vortices in the interior and a complicated flow structure, as displayed using VAPOR [26] in Fig. 6. Similar visualizations obtained at $p = 15$ are displayed in Fig. 7. See Supplemental Material at [27] for videos of the vorticity evolution for $p = 1$ and $p = 15$. Comparing these two cases, we see that at $t = 6$ the two visualizations are markedly different; the supplemental video at [27] shows that the difference can be seen starting at around $t = 5$. At later times, when thermalization occurs, the vortex tubes of Fig. 6d are dominated by fluctuations that take the form of *point blobs*, less elongated vorticity structures, as seen in Fig. 7d. This change of structure is best seen in Fig. 8, which shows visualizations of runs at resolution 1024^3 at $t = 9$ in a cubic subregion of width $\pi/3$ centered at $x = y = z = \pi/2$ for for $p = 1$ (a) and $p = 10$ (b). The vortex tubes that are clearly the dominant structure in the $p = 1$ case coexist in the $p = 10$ case with point blobs that resemble the structures that appear in visualizations of the truncated Euler equations in [28].

In figure 9 we show the probability distribution function of the vorticity along the x-direction for the same runs at the same time. The long tails that are present for the $p = 1$ simulation are suppressed for $p = 10$ since the system's behavior is closer to the Gaussian behavior

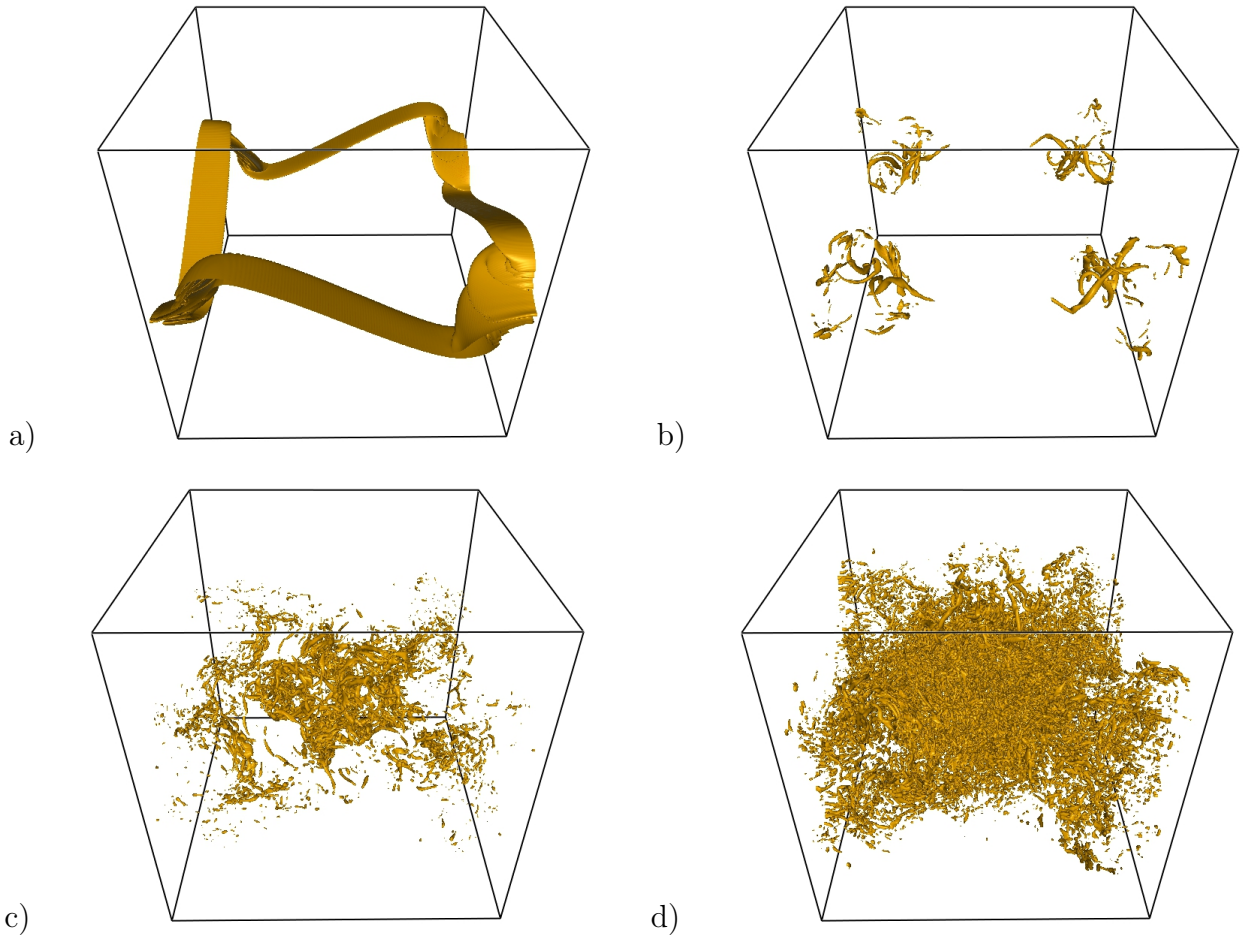

FIG. 7. Isosurfaces (at 12% of maximum) of square vorticity $\omega^2 = (\nabla \times \mathbf{v})^2$ at resolution 512^3 in the impermeable box, $p = 15$ and $t = 4$, 6, 8, 10.

expected for a thermalized state.

D. Thermalization and finite dissipation

Looking at the previous sections we have two apparently contradictory results. On the one hand, based on figure 2 there is finite energy dissipation that is independent of the value of p used. This indicates that this is an out-of-equilibrium dissipating system. On the other hand, the energy spectrum and structures resemble those of the thermalized absolute equilibrium state [16]. As discussed in the introduction, the thermalized state is realized in the truncated Euler equations, where a finite number of modes is kept and the energy is exactly conserved. Thus, if indeed there was a transition from the hyper-viscous Navier-Stokes equation to the truncated Euler equations, one would expect to see a suppression of the energy dissipation that is not observed here.

To resolve this discrepancy we recall the arguments in [6], in which the energy dissipation term in Fourier space is written as

$$-\nu_p k^{2p} \hat{\mathbf{u}}_\mathbf{k} = \frac{U}{L} \left(\frac{k}{k_{_G}} \right)^{2p} \hat{\mathbf{u}}_\mathbf{k} \tag{10}$$

where $\nu_p = U k_{_G}^{-2p} / L$ and $k_{_G}$ is a wavenumber in the dissipation range chosen off-lattice so that no wavenumber is exactly equal to $k_{_G}$. The limit $p \to \infty$ is then taken while keeping $k_{_G}$ fixed. This is similar to the procedure followed here, where we tuned ν_p so that the maximum of the dissipation spectrum is smaller but close to the maximum wavenumber allowed by our grid. In this case it is clear that, as $p \to \infty$, wavenumbers smaller than $k_{_G}$ will not feel the effect of viscosity while wavenumbers larger than k_G will be suppressed. The whole system will thus resemble the truncated Euler system with k_G acting as the truncation wavenumber. However for a finite p (if the Fourier wavenumbers are sufficiently dense) there will be wavenumbers close to k_G that will be effective at dissipating energy. To estimate the width of wavenumbers that effectively dissipate energy we consider the dissipation spectrum given by $D(k) = \nu_p k^{2p} E(k)$ and assume that at large k, the energy spectrum takes the form

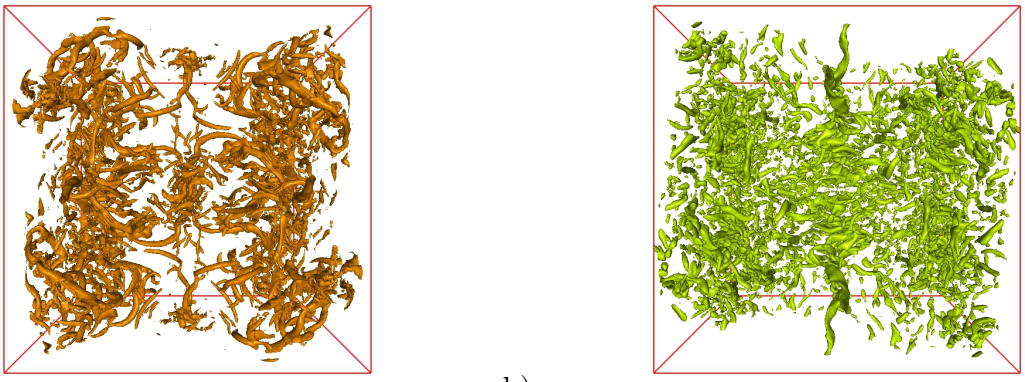

a) b)

FIG. 8. Enlargement of a cubic subregion of width $\pi/3$ centered at $x = y = z = \pi/2$ of isosurfaces of square vorticity $\omega^2 = (\nabla \times \mathbf{v})^2$ at resolution 1024^3 and $t = 9$. Left: $p = 1$ and isosurface at 10% of maximum; Right: $p = 10$ and isosurface at 20% of maximum.

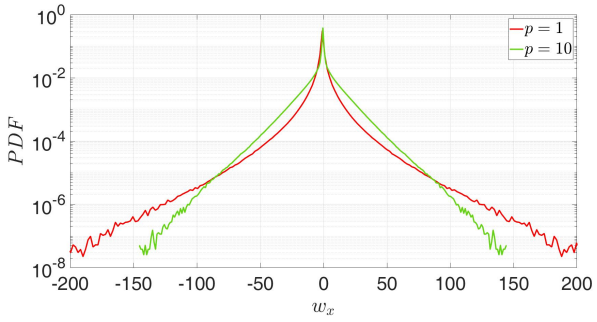

FIG. 9. Probability distribution function of the vorticity along the x-direction at the peak of the energy dissipation for the runs at resolution 1024^3 for $p = 1$ and $p = 10$. The distributions were computed inside the impermeable box, with the same conditions as in Fig. 8.

$E(k) \propto k^{\alpha_p} e^{-k/k_d}$. Therefore $D(k) \propto k^{2p+\alpha_p} e^{-k/k_d}$, the integral of which gives the energy dissipation rate ϵ. For large values of p, the dissipation spectrum is highly concentrated around a wavenumber k_* and the integral $\int D(k)dk = \epsilon$ can be estimated by writing

$$k^{2p+\alpha_p} e^{-k/k_d} = \exp\left[(2p + \alpha_p)\ln(k) - k/k_d\right] \qquad (11)$$

and using the steepest descent method. Expanding the argument of the exponential around its maximum value at $k_* = (2p + \alpha_p)k_d$ with $D(k_*) = D_* = \nu_p(k_*/e)^{2p+\alpha_p}$, we see that the dissipation spectrum can be approximated as

$$D(k) \simeq D_* \exp\left[-\frac{1}{2}\left(\frac{q}{k_*/\sqrt{2p+\alpha_p}}\right)^2\right] \qquad (12)$$

where $q = k - k_*$, i.e. as a Gaussian centered at k_* of width

$$\delta q \simeq \frac{k_*}{\sqrt{2p+\alpha_p}} \qquad (13)$$

In our simulations, we tuned ν_p so that the maximum of the dissipation spectrum at k_* remained fixed and close to the maximum wavenumber k_{max}. Therefore, the wavenumbers that dissipate effectively are those that are approximately within a distance of δq away from k_*.

For the dissipation to be suppressed, the width δq must be smaller than the spacing δk between two neighboring shells that contain at least one wavenumber in the discrete wavenumber space $\mathbf{k} \in \mathbb{N}^3$. In three dimensions, the spacing between neighbouring spherical shells of radius k is of the order $\delta k \simeq 1/k$. (To illustrate this point, we note that the closest spherical shell to the shell containing the wavenumber $\mathbf{k} = (0, 0, k)$ is that which contains the wavenumber $\mathbf{k'} = (1, 0, k)$ and has norm $k' = \sqrt{1 + k^2} \simeq k + \frac{1}{2}k^{-1} + \ldots$.) Equating δq obtained from the steepest descent method with $\delta k = k' - k$ we obtain that the system will behave like the truncated Euler equations and energy dissipation will be suppressed when $\delta q \ll \delta k$ which implies that

$$p \gg k_*^4. \qquad (14)$$

Given that k_* in our simulations is of the order $k_* \simeq 150$ for the 512^3 and $k_* \simeq 300$ for the 1024^3 simulation, it is clear why energy dissipation still persists in this system: the order p would have to be around 10^{10} to see a strong suppression of the energy dissipation. At p of order 50 and 100, the system can still effectively dissipate energy since there are many wavenumbers inside the dissipating shell.

What does change, however, as p is increased is the number of triads $\mathbf{k_1} + \mathbf{k_2} + \mathbf{k_3} = \mathbf{0}$ of interacting wavenumbers that can transfer energy inside the dissipating shell. This number is decreased drastically as δq becomes smaller. In contrast, the number of triads that redistribute energy among all wavenumbers and lead to the thermalized state remains fixed. The ratio of the two therefore becomes smaller as p is increased (because δq is decreased). This leads the system to a quasi-equilibrium state, in which the mean forward flux

of energy (caused by the triads that transfer energy to the dissipating wavenumber shell) is subdominant to the fluctuations caused by the remaining triads that redistribute energy among modes leading to a thermalized state. This behavior has been observed recently by two of the authors [29], who showed that the thermalized behavior can appear in forced and dissipated flows for the truncated Navier-Stokes system. It was shown that for a given injection rate as the viscosity is reduced, the system makes a transition to a quasi-equilibrium, with the appearance of a thermal spectrum, provided that $k_{max}\,\eta \ll 1$. A similar situation occurs in the present system, not because of the reduction in viscosity, but because the dissipation is limited to wavenumbers inside a thin spherical shell.

IV. CONCLUSION

In this work we have examined decaying turbulence initiated by a Taylor-Green vortex using hyper-viscous numerical simulations for a wide range of orders of the hyper-viscous parameter p. We have shown that it is possible to integrate the Navier-Stokes equations with hyper-viscosity of order p of 50 or 100, much higher than the values of 2 to 8 that have been previously studied [1–5, 7]. For all values of p that we examined, the evolution of the total energy and its dissipation rate remained unaffected by the hyperviscosity and close to those of high-resolution $p = 1$ runs. The spectra and the structures remain unaltered up to $t = 5$, where almost inviscid dynamics are followed. At later times, however, the structures and the spectra diversify with the order of p. Even at these later times, the low-wavenumber portion of the spectra is surprisingly insensitive to the value of p even for high values of p, but the inertial range (the part of the spectrum that displays a $k^{-5/3}$ scaling) does not extend to indefinitely high k. As the order p is increased, a stronger bottleneck forms and the spatial structures change from vortex tubes to a mixture of vortex tubes and point blobs. Further studies would shed light on the nature of high-p hyper-viscosity, now that we have demonstrated its practical feasibility.

The main focus of this work was on the turbulent behavior at increasingly large values of p and attempted to make the connection between the bottleneck effect that is present in the usual Navier-Stokes equation and the thermalization of the flow that develops in the truncated Euler equations. We showed that as the hyper-viscosity order p is increased, the energy spectrum approaches that of the thermalized state of the truncated Euler equations of Kraichnan [16]. This transition was predicted in [6] by arguing that the hyper-viscous Navier-Stokes equations approach the truncated Euler equations as p goes to infinity. This is the first time that this transition has been demonstrated in simulations of three-dimensional turbulence.

Nonetheless for the hyper-viscous flow a finite dissipation rate independent of the value of p persists, contrary to the situation for the truncated Euler system. We argued that this behavior is due to the fact that for our grid resolutions and values of p, energy dissipation in Fourier space is concentrated in a spherical shell of width $\delta q \propto k_*/\sqrt{2p}$ that is thin but still much wider than the spacing between spherical wavenumber shells. Suppression of the energy dissipation was estimated to occur at much larger values of p.

In conclusion, a relationship has been established between the bottleneck in turbulence and flows in thermal equilibrium. Our work has also demonstrated a continuous way to pass from the Kolmogorov spectrum to a thermalized spectrum. Unlike other systems that have demonstrated such a transition [29–31], this path does not involve a discontinuous Galerkin truncation. Future work could include the forced Taylor-Green vortex and randomly forced flows for which long statistical averages can be performed that can shed further light in the transition from equilibrium to out of equilibrium dynamics.

V. ACKNOWLEDGMENTS

The numerical simulations were performed using high performance computing resources provided by the Institut du Developpement et des Ressources en Informatique Scientifique (IDRIS) of the Centre National de la Recherche Scientifique (CNRS), coordinated by GENCI (Grand Equipement National de Calcul Intensif) through grants A0050506421 and A0062A01119. This work was also granted access to the HPC resources of MesoPSL financed by the Region Ile de France and the project Equip@Meso (reference ANR-10-EQPX-29-01) of the programme Investissements d'Avenir supervised by the Agence Nationale pour la Recherche. This work was also supported by the Agence Nationale pour la Recherche via ANR DYSTURB project No. ANR-17-CE30-0004.

Appendix A: Time-integration scheme

We use an explicit second-order Runge-Kutta method to integrate the nonlinear advective terms of the Navier-Stokes equations. The linear viscous terms are often integrated via an implicit method, in order to increase the timestep from that imposed by the viscous stability requirement. As the Reynolds number increases, this constraint becomes less important than that imposed by the integration of the advective terms, and hence explicit timestepping is sometimes used for high Reynolds number simulations. However, the use of hyperviscosity poses a greater constraint on the timestep than ordinary viscosity. An analogous problem occurs in integrating the Kuramoto-Sivashinsky equation, which contains a fourth-order spatial derivative and has led to the use of an exponential scheme and the formulation of a modified exponential scheme called the slaved scheme [18].

Here we compare explicit timesetepping with exponential and modified exponential timestepping for treating the hyperviscous terms.

To describe the exponential methods, we write the evolution equation for a mode with wavenumber k schematically as

$$\partial_t u = -\nu k^{2p} u + \mathcal{N}(u) \tag{A1}$$

where $\mathcal{N}$ includes both the advective terms and the pressure projection. Equation (A1) can be rewritten as an integral equation

$$u(t+\Delta t) = e^{-\nu k^{2p}\Delta t} u(t) + \int_t^{t+\Delta t} d\tau\; e^{-\nu k^{2p}(t+\Delta t-\tau)} \mathcal{N}(u(\tau)) \tag{A2}$$

A first approximation, usually called time-splitting, is to set $\mathcal{N}(u(\tau)) \approx \mathcal{N}(u_N(\tau))$, where u_N is the result of integrating $\partial_t u_N = \mathcal{N}(u_N)$ from initial condition $u(t)$, here by the second-order Runge-Kutta scheme, i.e.

$$\begin{aligned}\int_t^{t+\Delta t} d\tau\, \mathcal{N}(u(\tau)) &\approx \int_t^{t+\Delta t} d\tau\, \mathcal{N}(u_N(\tau)) \\ &\approx u_N(t+\Delta t) - u(t)\end{aligned} \tag{A3}$$

The exponential $e^{-\nu k^{2p}(t+\Delta t-\tau)}$ in the integrand of (A2) is approximated by a single value, either its value at one point or by its average value. The commonly used scheme

$$u(t+\Delta t) \approx e^{-\nu k^{2p}\Delta t} u_N(t+\Delta t) \tag{A4}$$

is equivalent to evaluating the exponential at the left endpoint. Evaluating the exponential at the midpoint leads to the scheme

$$\begin{aligned}u(t+\Delta t) \approx\; & e^{-\nu k^{2p}\Delta t} u(t) \\ & + e^{-\nu k^{2p}\Delta t/2} \left(u_N(t+\Delta t) - u(t)\right)\end{aligned} \tag{A5}$$

The modified exponential, or slaved, method approximates the exponential in the integral by its average value, leading to the scheme

$$\begin{aligned}u(t+\Delta t) \approx\; & e^{-\nu k^{2p}\Delta t} u(t) \\ & + \frac{1 - e^{-\nu k^{2p}\Delta t}}{\nu k^{2p}\Delta t} (u_N(t+\Delta t) - u(t))\end{aligned} \tag{A6}$$

where the fraction in (A6) is evaluated as 1 if $\nu k^{2p}\Delta t$ is less than 10^{-5}.

The slaved scheme (A6) has the interesting property that it is exact for all Δt in the special case that $\mathcal{N}(u)$ is a constant $\mathcal{N}$. A generalization of this argument shows that if $\mathcal{N}(u)$ varies slowly compared with the timescale $1/(\nu k^{2p})$, then scheme (A6) is accurate even for large Δt.

In our case, the timestep is limited by the Runge-Kutta integration of the nonlinear term. We use $\Delta t = 0.001$, for which the midpoint exponential scheme (A5) and the slaved scheme (A6) both yield satisfactory results. For these timesteps, the left endpoint exponential scheme (A4) is less accurate and the explicit scheme diverges.

[1] Vadim Borue and Steven A Orszag, "Forced three-dimensional homogeneous turbulence with hyperviscosity," Europhys. Lett. **29**, 687 (1995).

[2] Vadim Borue and Steven A Orszag, "Numerical study of three-dimensional Kolmogorov flow at high Reynolds numbers," J. Fluid Mech. **306**, 293–323 (1996).

[3] Victor S L'vov, Itamar Procaccia, and Damien Vandembroucq, "Universal scaling exponents in shell models of turbulence: viscous effects are finite-sized corrections to scaling," Phys. Rev. Lett. **81**, 802 (1998).

[4] Nils Erland L Haugen and Axel Brandenburg, "Inertial range scaling in numerical turbulence with hyperviscosity," Phys. Rev. E **70**, 026405 (2004).

[5] A.G. Lamorgese, D.A. Caughey, and SB Pope, "Direct numerical simulation of homogeneous turbulence with hyperviscosity," Phys. Fluids **17**, 015106 (2005).

[6] Uriel Frisch, Susan Kurien, Rahul Pandit, Walter Pauls, Samriddhi Sankar Ray, Achim Wirth, and Jian-Zhou Zhu, "Hyperviscosity, Galerkin truncation, and bottlenecks in turbulence," Phys. Rev. Lett. **101**, 144501 (2008).

[7] Kyle Spyksma, Moriah Magcalas, and Natalie Campbell, "Quantifying effects of hyperviscosity on isotropic turbulence," Phys. Fluids **24**, 125102 (2012).

[8] Samriddhi Sankar Ray, "Thermalized solutions, statistical mechanics and turbulence: An overview of some recent results," Pramana **84**, 395–407 (2015).

[9] Uriel Frisch, Samriddhi Sankar Ray, Ganapati Sahoo, Debarghya Banerjee, and Rahul Pandit, "Real-space manifestations of bottlenecks in turbulence spectra," Phys. Rev. Lett. **110**, 064501 (2013).

[10] Debarghya Banerjee and Samriddhi Sankar Ray, "Transition from dissipative to conservative dynamics in equations of hydrodynamics," Phys. Rev. E **90**, 041001(R) (2014).

[11] Gregory Falkovich, "Bottleneck phenomenon in developed turbulence," Phys. Fluids **6**, 1411–1414 (1994).

[12] Detlef Lohse and Axel Müller-Groeling, "Bottleneck effects in turbulence: Scaling phenomena in r versus p space," Phys. Rev. Lett. **74**, 1747 (1995).

[13] D.O. Martinez, S Chen, G.D. Doolen, R.H. Kraichnan, L.P. Wang, and Y Zhou, "Energy spectrum in the dissipation range of fluid turbulence," J. Plasma Phys. **57**, 195–201 (1997).

[14] D.A. Donzis and K.R. Sreenivasan, "The bottleneck effect and the Kolmogorov constant in isotropic turbulence," J. Fluid Mech. **657**, 171–188 (2010).

[15] Christian Küchler, Gregory Bewley, and Eberhard Bodenschatz, "Experimental study of the bottleneck in fully developed turbulence," J. Stat. Phys. **175**, 617–639 (2019).

[16] Robert H Kraichnan, "Helical turbulence and absolute equilibrium," J. Fluid Mech. **59**, 745–752 (1973).

[17] M. E. Brachet, M. D. Bustamante, G Krstulovic, Pablo Daniel Mininni, A Pouquet, and D Rosenberg, "Ideal evolution of magnetohydrodynamic turbulence when imposing Taylor-Green symmetries," Phys. Rev. E **87**, 013110 (2013).

[18] Uriel Frisch, Zhen Su She, and Olivier Thual, "Viscoelastic behaviour of cellular solutions to the Kuramoto-Sivashinsky model," J. Fluid Mech. **168**, 221–240 (1986).

[19] G.I. Taylor and A.E. Green, "Mechanism of the production of small eddies from large ones," Proc. Roy. Soc. A **158**, 499–521 (1937).

[20] S. Douady, Y. Couder, and M. E. Brachet, "Direct observation of the intermittency of intense vorticity filaments in turbulence," Phys. Rev. Lett. **67**, 983–986 (1991).

[21] S Fauve, C Laroche, and B Castaing, "Pressure-fluctuations in swirling turbulent flows," J. Physique II **3**, 271–278 (1993).

[22] J Maurer, P Tabeling, and G Zocchi, "Statistics of turbulence between two counter-rotating disks in low-temperature helium gas," Europhys. Lett. **26**, 31–36 (1994).

[23] M. E. Brachet, Daniel I. Meiron, Steven A. Orszag, B. G. Nickel, Rudolf H. Morf, and Uriel Frisch, "Small–scale structure of the Taylor-Green vortex," J. Fluid Mech. **130**, 411–452 (1983).

[24] E. Lee, M. E. Brachet, A. Pouquet, P. D. Mininni, and D. Rosenberg, "Paradigmatic flow for small-scale magnetohydrodynamics: Properties of the ideal case and the collision of current sheets," Phys. Rev. E **78**, 066401 (2008).

[25] A. Pouquet, E. Lee, M. E. Brachet, P. D. Mininni, and D. Rosenberg, "The dynamics of unforced turbulence at high Reynolds number for Taylor-Green vortices generalized to MHD," Geophys. Astrophys. Fluid Dyn. **104**, 115–134 (2010).

[26] J. Clyne, P. Mininni, A. Norton, and M. Rast, "Interactive desktop analysis of high resolution simulations: application to turbulent plume dynamics and current sheet formation," New J. Phys. **9**, 301 (2007).

[27] URL will be inserted by publisher.

[28] Alexandros Alexakis and M. E. Brachet, "On the thermal equilibrium state of large-scale flows," J. Fluid Mech. **872**, 594–625 (2019).

[29] Alexandros Alexakis and M. E. Brachet, "Energy fluxes in quasi-equilibrium flows," J. Fluid Mech. **884**, A33 (2020).

[30] Vishwanath Shukla, Bérengère Dubrulle, Sergey Nazarenko, Giorgio Krstulovic, and Simon Thalabard, "Phase transition in time-reversible Navier-Stokes equations," Phys. Rev. E **100**, 043104 (2019).

[31] Luca Biferale, Massimo Cencini, Massimo De Pietro, Giovanni Gallavotti, and Valerio Lucarini, "Equivalence of nonequilibrium ensembles in turbulence models," Phys. Rev. E **98**, 012202 (2018).